CHAPTER 4

IMPLEMENTATION OF OBSERVER DESIGN TO CSTRs

4.1 INTRODUCTION

FKF, EKF and ASFKF designs discussed in chapter 3 are used in this chapter to estimate the states of CSTRs. The performance of FKF and EKF are compared.

4.2 PROCESS DESCRIPTION

4.2.1 Continuous Stirred Tank Reactor (CSTR- I)

The first principles model of the CSTR-I system and the operating point data (Refer Table 4.1) as specified in the paper titled Fuzzy Model Predictive Control by Huang et al (2000) have been used in the simulation studies. Highly nonlinear CSTR process is very common in chemical and petrochemical plants. In the process considered for simulation study as shown in Figure 4.1, an irreversible, exothermic reaction A → B occurs in constant volume reactor that is cooled by a single coolant stream. The CSTR-I process is modeled by the following equations:

$$\frac{dC_A(t)}{dt} = \frac{q(t)}{V}\left(C_{AO}(t) - C_A(t)\right) - K_O C_A(t) \exp\left(\frac{-E}{RT(t)}\right) \qquad (4.1)$$

$$\frac{dT(t)}{dt} = \frac{q(t)}{V}\left(T_O(t) - T(t)\right) - \frac{(-\Delta H)K_0 C_A(t)}{\rho C_p}\exp\left(\frac{-E}{RT(t)}\right) + \frac{\rho_c C_{pc}}{\rho C_p V} q_c(t) * \\ * \left\{1 - \exp\left(\frac{-hA}{q_c(t)\rho C_p}\right)\right\}\left(T_{co}(t) - T(t)\right) \quad (4.2)$$

Table 4.1 Steady state operating data of CSTR - I

Process variables	**Normal operating condition**
Measured product concentration (C_A)	0.0989 mol/l
Reactor temperature (T)	438.773 K
Coolant flow rate (q_c)	103 l/min
Process flow rate (q)	100 l/min
Feed concentration (C_{AO})	1 mol/l
Feed temperature (T_O)	350 K
Inlet coolant temperature (T_{co})	350 K
CSTR volume (V)	100 l
Heat transfer term (hA)	7×10^5 cal/(min K)
Reaction rate constant (K_O)	$7.2 \times 10^{10} min^{-1}$
Activation energy term $\left(\frac{E}{R}\right)$	1×10^4 K
Heat of reaction $(-\Delta H)$	-2×10^5 cal/mol
Liquid density (ρ, ρ_c)	1×10^3 g/l
Specific heats (C_p, C_{pc})	1 cal/(g.k)

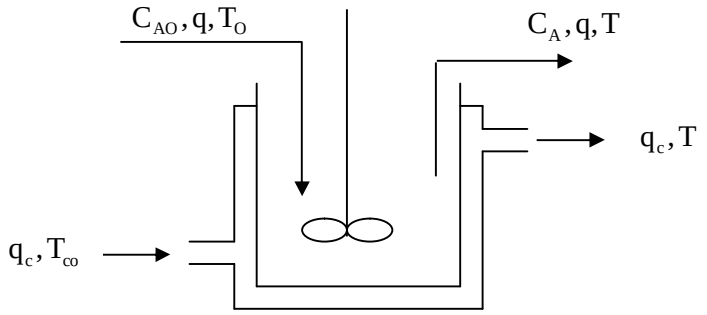

Figure 4.1 CSTR – I

The state x(t) and input u(t) vectors are given by $\mathbf{x}(t) = \begin{bmatrix} C_A \\ T \end{bmatrix}$ and $u(t) = [q_c]$ .The continuous linear state space model is obtained by linearizing the differential equations (4.1 and 4.2) around the nominal operating point (C_{As} and T_s) and is given by:

$$\tilde{\mathbf{x}} = A\tilde{\mathbf{x}} + B\tilde{u} \tag{4.3}$$

$$\tilde{y} = C\tilde{x} \tag{4.4}$$

$$A = \begin{pmatrix} A_{11} & A_{12} \\ A_{21} & A_{22} \end{pmatrix}$$

where

$$A_{11} = -\frac{q}{V} - k_s$$

$$A_{12} = -C_{AS} k_{ss}$$

$$A_{21} = -\left(\frac{\Delta h}{\rho C_\rho}\right) k_s$$

$$A_{22} = \left(-\frac{q}{V}\right) - \left(\frac{\Delta H C_{AS}}{\rho C_p}\right) k_{ss} + \left(-\frac{\rho_c C_{pc}}{\rho C_p V}\right) q_c + \left(\frac{\rho_c C_{pc}}{\rho C_p V}\right) q_c \exp\left(\frac{-hA}{q_c \rho C_p}\right)$$

$$\text{where } k_s = k_o \exp\left(-\frac{E}{RT_S}\right)$$

$$k_{ss} = k_0 \exp\left(-\frac{E}{RT_S}\right)\left(\frac{E}{RT_S^2}\right)$$

$$B = \begin{pmatrix} B_1 \\ B_2 \end{pmatrix}$$

where

$$B_1 = 0$$

$$B_2 = a_3 + a_3 q_c \exp\left(\frac{a_1}{q_c}\right)\left(\frac{a_1}{q_c^2}\right) - a_3 \exp\left(\frac{a_1}{q_c}\right) a_2$$

$$\text{where } a_1 = -\frac{hA}{\rho C_p}\ ,\ a_2 = T_{c0} - T_S,\ a_3 = \frac{\rho_c C_{pc}}{\rho C_p V}$$

$$C = \begin{bmatrix} 0 & 1 \end{bmatrix} \quad (\text{if } T \text{ alone is measurable})$$

$$C = \begin{bmatrix} 1 & 0 \\ 0 & 1 \end{bmatrix} \quad (\text{if both } C_A \text{ and } T \text{ are measurable})$$

Where matrices A, B represent the Jacobians corresponding to the nominal values of the state variables and input variables and $\tilde{x}$, $\tilde{u}$ and $\tilde{y}$ represent the deviation variables.

4.2.2 Continuous Stirred Tank Reactor (CSTR-II)

The first principles model of the CSTR-II (Refer Figure 4.2) and the operating point data (Refer Table 4.2) as specified in the book titled Process Control by Wayne Bequette (2003) have been used in the simulation studies. In this CSTR-II, for simplicity, it is assumed that the cooling jacket temperature can be directly manipulated, so that an energy balance around the jacket is not required. The process is modeled by the following Equations (4.5 and 4.6) (Bequette 2002, 2003 and Raymond 2006).

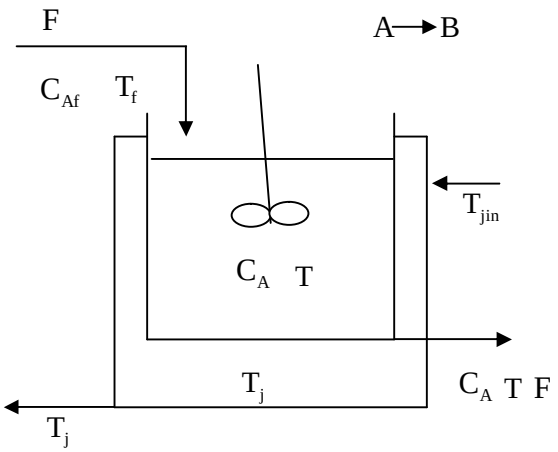

Figure 4.2 CSTR – II

Table 4.2 Steady state operating data of CSTR-II

Process Variable	Normal Operating Condition
Volumetric flow rate/ Reactor volume $\frac{F}{V}, hr-1$	1
Pre-exponential factor $K_0, hr-1$	9,703*3600
Heat of reaction $(-\Delta H), kcal/kgmol$	5960
Activation energy $(E_a), kcal/kgmol$	11843
Density x Heat capacity $\rho C_p, kcal/m^3\ ^0C$	500
Feed temperature $T_f\ ^0C$	25
Concentration of A in feed stream $C_{Af}, kgmol/m^3$	10
$\frac{\text{Overall heat transfer coefficient x Area for heat exchanger}}{\text{Volume}}$ $\frac{UA}{V}, kcal/m^{3\,0}C$	150
Jacket temperature $T_j\ ^0C$	25

$$\frac{dC_A}{dt} = \frac{F}{V}\left(C_{Af} - C_A\right) - K_0 \exp\left(\frac{-E_a}{RT}\right) C_A \tag{4.5}$$

$$\frac{dT}{dt} = \frac{F}{V}\left(T_f - T\right) + \frac{-\Delta H}{\rho C_P} K_0 \exp\left(\frac{-E_a}{RT}\right) C_A - \frac{UA}{V\rho C_P}\left(T - T_j\right) \tag{4.6}$$

The state x(t) and input u(t) vectors are given by $x(t) = \begin{bmatrix} C_A \\ T \end{bmatrix}$ and $u(t) = \begin{bmatrix} T_j \end{bmatrix}$. The continuous linear state space model (Refer Equations 4.3 and 4.4) is obtained by linearizing the differential equations (4.5 and 4.6) around the nominal operating point (C_{As} and T_s) and is given by

$$A = \begin{bmatrix} \frac{-F}{V} - K_s & -C_{As}K_s' \\ \frac{(-\Delta H)}{\rho C_p} K_s & \frac{-F}{V} - \frac{UA}{V\rho C_p} + \frac{(-\Delta H)}{\rho C_p} C_{As} k_S' \end{bmatrix}$$

$$B = \begin{bmatrix} 0 \\ \frac{UA}{V\rho C_p} \end{bmatrix} \qquad C = \begin{bmatrix} 1 & 0 \\ 0 & 1 \end{bmatrix}$$

$$D = \begin{bmatrix} 0 \end{bmatrix}$$

where

$$K_s = K_0 \exp\left(\frac{-\Delta E}{RT_s}\right)$$

$$K_s' = K_0 \exp\left(\frac{-\Delta E}{RT_s}\right)\left(\frac{\Delta E}{RT_s^2}\right)$$

4.2.3 Multiple steady state characteristics (CSTR-II)

If we start at a low jacket temperature, the reactor operates at a low temperature (point 1). As the jacket temperature is increased, the reactor temperature increases (points 2 and 3) until the low temperature limit point

(point 4) is reached. If the jacket temperature is slightly increased further, the reactor temperature jumps (ignites) to a high temperature (point 8); any further increase in jacket temperature result in slight increase in reactor temperature as shown in Figure 4.3.

If we start at a high jacket temperature (point 9), there is a single high reactor temperature, which decreases as the jacket temperature is decreased (points 8 and 7). As we move slightly to point which is lower than the high temperature limit point (point 6), the reactor temperature drops (also known as extinction) to a low temperature (point 2). Further decreases in jacket temperature lead to small decrease in reactor temperature.

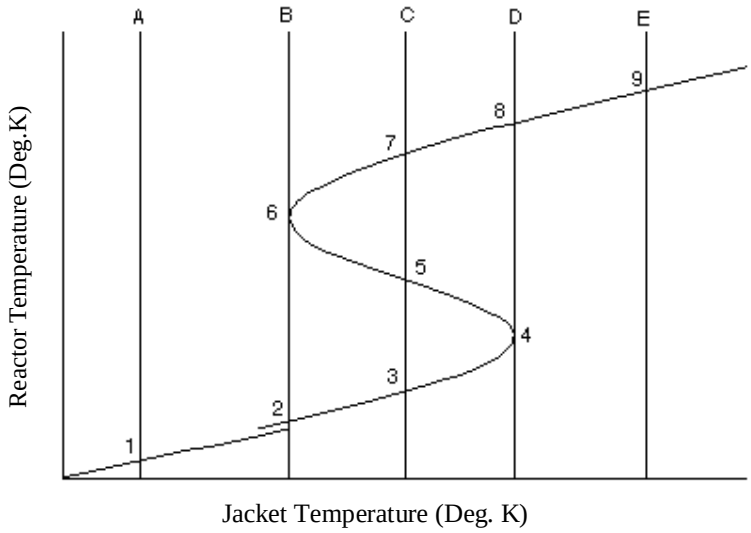

Figure 4.3 Reactor temperature vs. Jacket temperature of CSTR-II

In CSTR-II there are two stable operating points at low and high temperature (311.2 Deg. K. and 368.1 Deg. K.) respectively and one unstable operating point in middle (339.1 Deg. K.).

4.3 OBSERVER FOR CSTR-I

FKF, ASFKF and EKF design procedures as discussed in chapter 3 are applied to CSTR-I to estimate the concentration and temperature. The dynamic behaviour of the CSTR process is not the same at different operating points, and the process is, indeed, nonlinear. To verify this fact, the nonlinear system has been linearized at different operating points (see Table 4.3). The damping factor and undamped natural frequency have been obtained at different operating points and are reported in Table 4.3. From this Table, it can be inferred that the process is highly nonlinear, because there is significant variation in the damping factor and undamped natural frequency.

Table 4.3 Eigen values, damping factor and undamped natural frequency at different operating points

Operating Point	Eigen value	Damping factor	Freq. (rad/s)
At q_c=97 $\bar{C}_A = 0.0795$ $\bar{T} = 443.4566$	-2.5967 ± 2.9463i	0.661	3.93
At q_c=100 $\bar{C}_A = 0.0885$ $\bar{T} = 441.1475$	-1.9641 ± 3.0590i	0.540	3.64
At q_c=103 $\bar{C}_A = 0.0989$ $\bar{T} = 438.7763$	-1.3886 ± 3.0366i	0.395	3.29
At q_c=106 $\bar{C}_A = 0.1110$ $\bar{T} = 436.3091$	-0.8632 ± 2.9083 i	0.285	3.03
At q_c=109 $\bar{C}_A = 0.1254$ $\bar{T} = 433.6921$	-0.3810 ± 2.6843i	0.141	2.71

Figures 4.5 and 4.6 show the comparison of the open-loop responses of the linear model developed around a nominal operating point values (Refer Table 4.1) with the rigorous model in the presence of the coolant flow rate variation as shown in Figure 4.4. From the response, it can be concluded that the linear model developed around a nominal operating point is not able to capture the dynamics (oscillatory behavior) of the CSTR-I process adequately. Hence, it is necessary to represent the nonlinear system using the T-S fuzzy model.

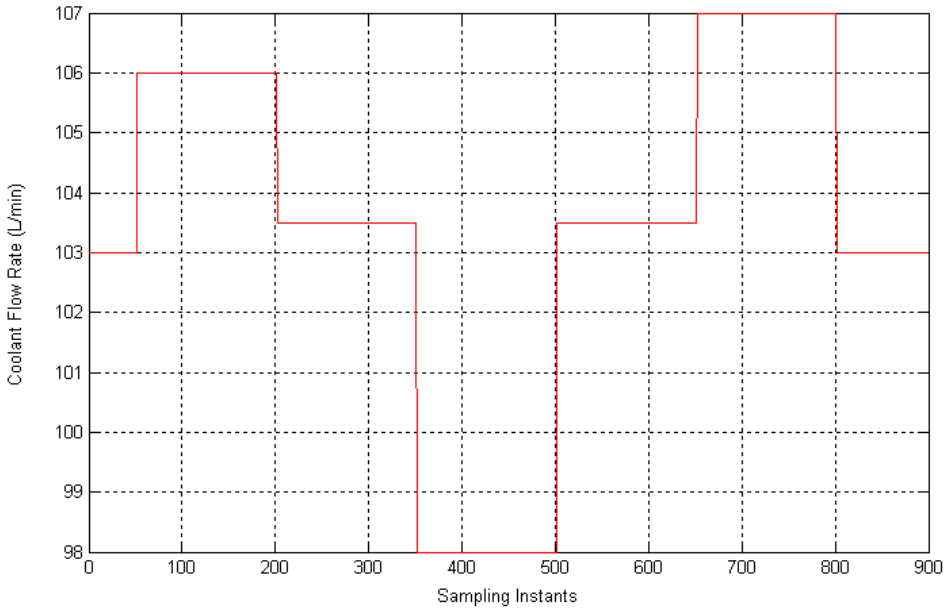

Figure 4.4 Variation in coolant flow rate of CSTR-I

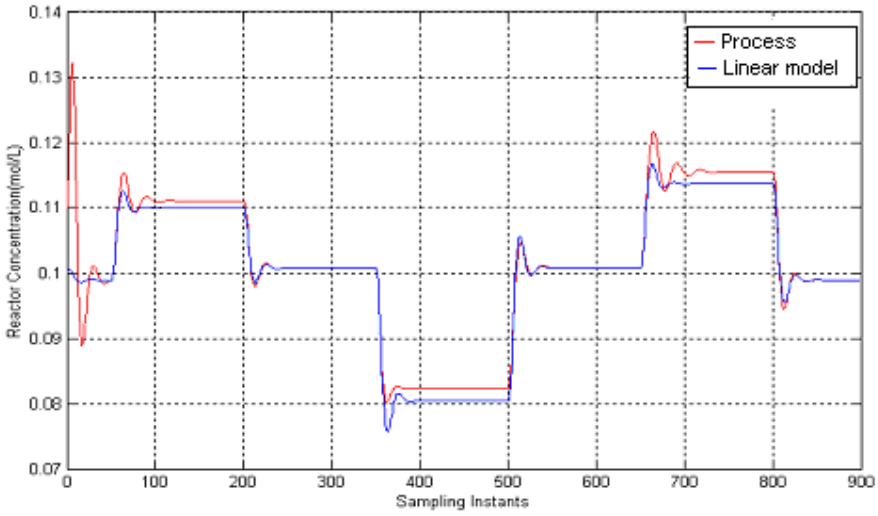

Figure 4.5 Comparison of the open loop responses of rigorous model and linear model of CSTR-I - Reactor Concentration

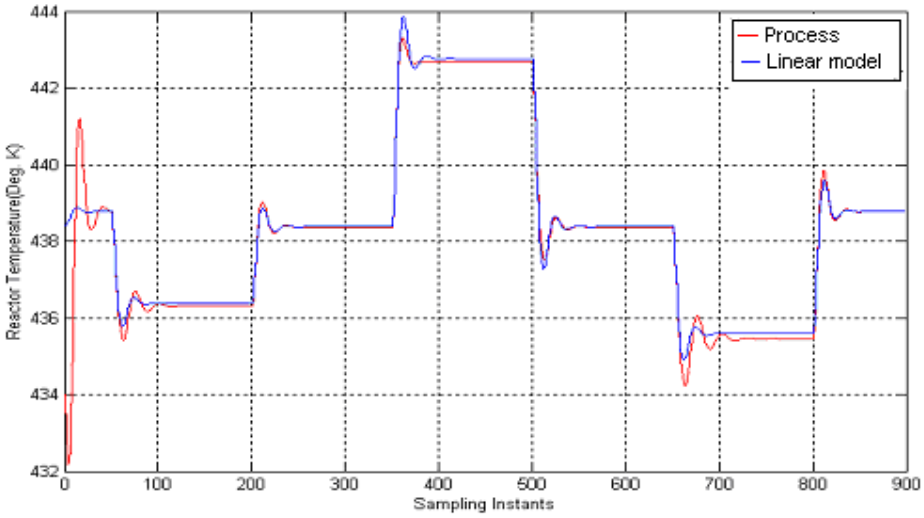

Figure 4.6 Comparison of the open loop responses of rigorous model and linear model of CSTR-I - Reactor Temperature

4.3.1 Fuzzy model for CSTR-I process

The T-S fuzzy model is based on multiple local linear state space models that are weighted using fuzzy membership function. In the T-S fuzzy model the rule premises can be considered as an input space partitioning and the rule consequences as local models, valid in the rule's partition. To combine multiple local linear state space models one must devise a method for partitioning the operating state space. The choice of variables to be used to characterize the operating regimes are highly problem dependent Johansen (1997). We observed that the dynamic behaviour of the CSTR-I system changes significantly depending on the operating point. Therefore, the coolant flow rate (premise variable) has been selected to partition the operating space of the CSTR-I system. In order to express smooth transitions between adjacent regimes, the domain of each operating regime is characterized by a fuzzy set membership function. The shape of the membership function has been selected in such a way that the weight for the model i will be equal to 1 if operated exactly at the point at which the model has been devised. If the input value is between two linearization points, the output will consider only the two associated linear models which imply that the rest of the membership function must have a value of zero.

As suggested by Schott and Bequette (1997), we have selected the number of local models to be equal to that of the number of operating regimes over which the system is expected to operate. Further, each local model parameters (consequent part of T-S fuzzy model) is determined by linearizing the nonlinear differential equation (4.1 and 4.2) at different operating points.

In this work, we have intended to interpolate five models that have been generated at five different operating points. Because the operating space has been partitioned on a single parameter (coolant flow rate), there are only

five rules in the rule base. The universe of discourse is divided into five intervals which are defined by the linguistic variables very low, low, medium, high and very high respectively. Figure 4.7 shows the triangular membership functions that are used to partition the input space q_c.

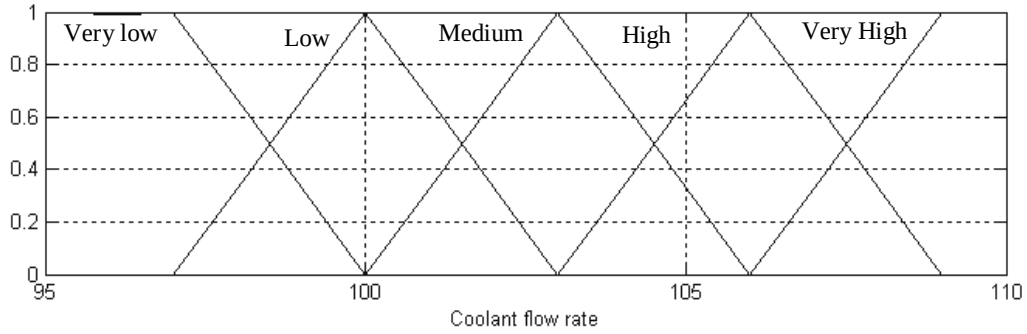

Figure 4.7 Membership function

The linear time invariant discrete state space models (Refer Equations 3.25 and 3.26) for five different operating points of CSTR - I are:

Operating point: 1 ($q_c = 97$ $\bar{C}_A = 0.0795$ and $\bar{T} = 443.4566$)

$$\Phi_1 = \begin{bmatrix} 1.2040\text{e-}001 & -3.1008\text{e-}003 \\ 1.5350\text{e+}002 & 1.4438 \end{bmatrix} \quad \Gamma_1 = \Psi_1 = \begin{bmatrix} 1.2927\text{e-}004 \\ -9.6293\text{e-}002 \end{bmatrix}$$

Operating point: 2 ($q_c = 100$, $\bar{C}_A = 0.0885$ and $\bar{T} = 441.1475$)

$$\Phi_2 = \begin{bmatrix} 1.7133\text{e-}001 & -3.2672\text{e-}003 \\ 1.4362\text{e+}002 & 1.4733 \end{bmatrix} \quad \Gamma_2 = \Psi_2 = \begin{bmatrix} 1.3035\text{e-}004 \\ -9.4559\text{e-}002 \end{bmatrix}$$

Operating point: 3 ($q_c = 103$, $\bar{C}_A = 0.0989$ and $\bar{T} = 438.7763$)

$$\Phi_3 = \begin{bmatrix} 2.2479\text{e-}001 & -3.4252\text{e-}003 \\ 1.3333\text{e+}002 & 1.5012 \end{bmatrix} \quad \Gamma_3 = \Psi_3 = \begin{bmatrix} 1.3074\text{e-}004 \\ -9.2643\text{e-}002 \end{bmatrix}$$

Operating point: 4 (q_c =106, $\bar{C}_A$ =0.1110 and $\bar{T}$= 436.3091)

$$\Phi_4 = \begin{bmatrix} 2.8071e\text{-}001 & -3.5731e\text{-}003 \\ 1.2254e{+}002 & 1.5270 \end{bmatrix} \quad \Gamma_4 = \Psi_4 = \begin{bmatrix} 1.3038e\text{-}004 \\ -9.0506e\text{-}002 \end{bmatrix}$$

Operating point: 5 (q_c =109 , $\bar{C}_A$ =0.1254 and $\bar{T}$=433.6921))

$$\Phi_5 = \begin{bmatrix} 3.3941e\text{-}001 & -3.7084e\text{-}003 \\ 1.1123e{+}002 & 1.5504 \end{bmatrix} \quad \Gamma_5 = \Psi_5 = \begin{bmatrix} 1.2913e\text{-}004 \\ -8.8085e\text{-}002 \end{bmatrix}$$

$C = \begin{bmatrix} 0 & 1 \end{bmatrix}$ (if T alone is measurable) for i=1:5

$C = \begin{bmatrix} 1 & 0 \\ 0 & 1 \end{bmatrix}$ (if both C_A and T are measurable) for i=1:5

Figures 4.8 and 4.9 show the rigorous model and fuzzy model responses for step changes in the coolant flow rate q_c (Refer Figure 4.4) and in the presence of the following initial conditions:

$C_A = 0.11$ and $\hat{C}_A = 0.1$

.

$T = 434$ and $\hat{T} = 438.44$

From the response, it is evident that the fuzzy model is able to capture the dynamics of CSTR-I process perfectly. It should be noted that the process is simulated using the nonlinear first principles model (Refer Equations 4.1 and 4.2).

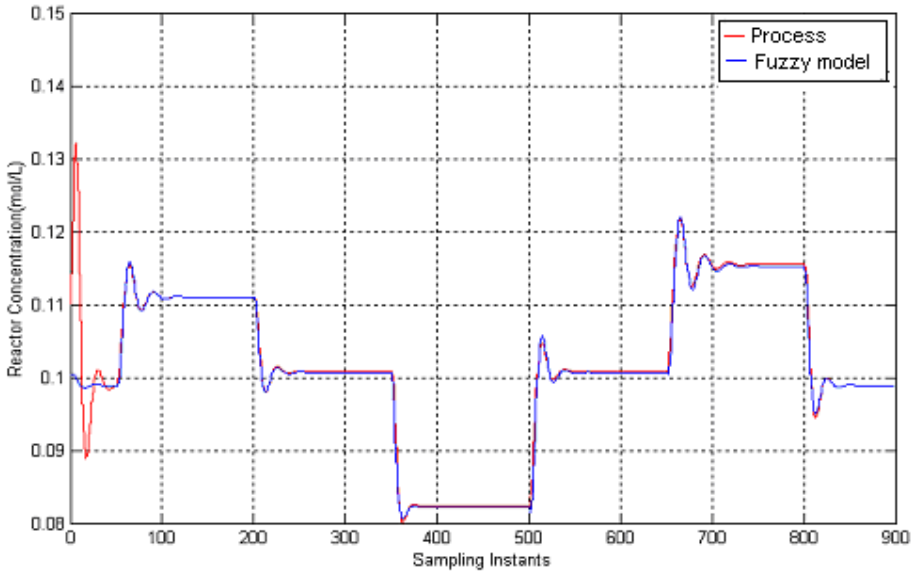

Figure 4.8 Comparison of the open loop responses of rigorous model and fuzzy model of CSTR-I - Reactor Concentration

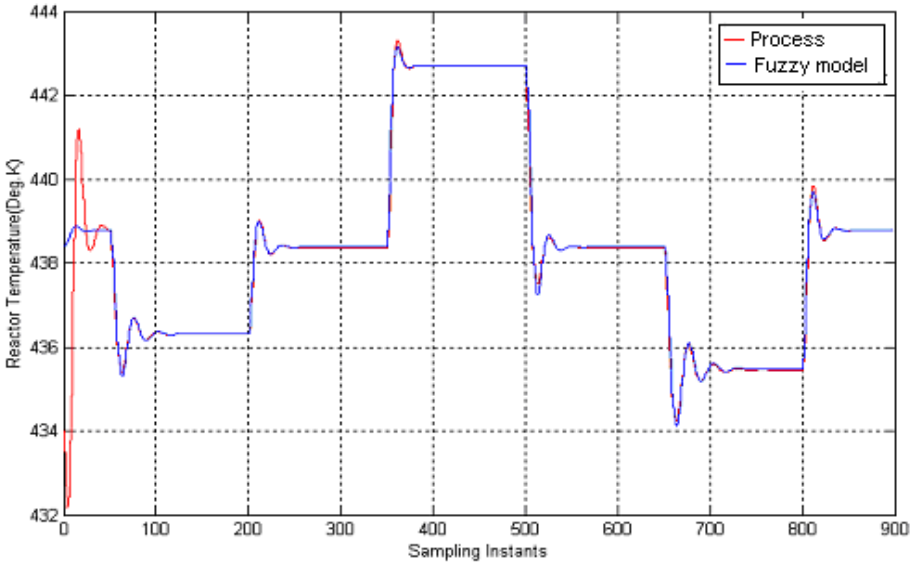

Figure 4.9 Comparison of the open loop responses of rigorous model and fuzzy model of CSTR-I - Reactor Temperature

4.3.2 FKF for CSTR-I process

The performance of the FKF, when only the reactor temperature alone is measured, is shown in Figures 4.10 and 4.11. We have assumed that the random errors are present in the measurement (T) as well as in the coolant flow rate (q_c). The covariance matrices of measurement noise and state noise are assumed as

$$R = [0.05)^2] \quad \text{and} \quad Q = \left[(0.05)^2\right]$$

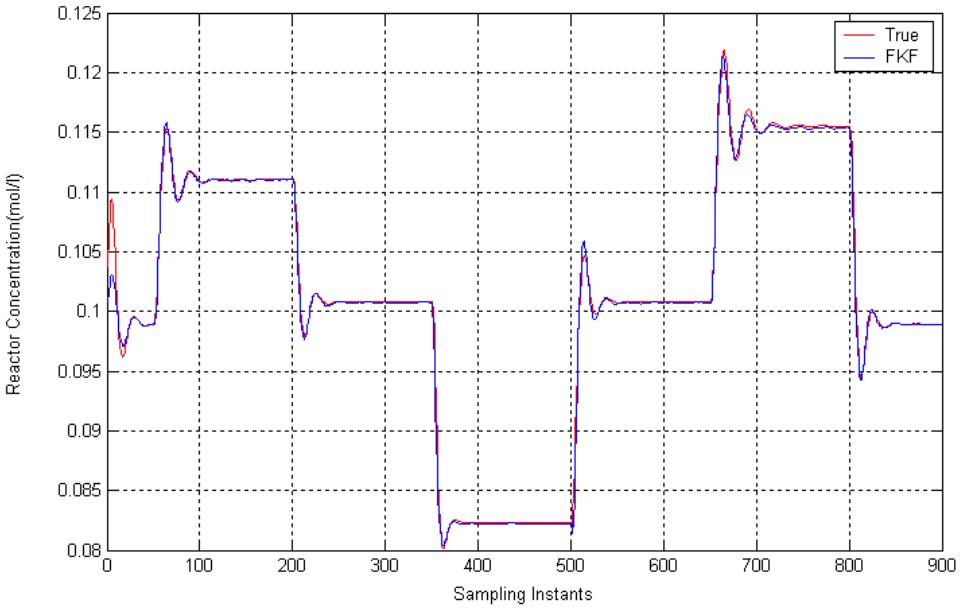

Figure 4.10 Evolution of true and estimated reactor concentration of CSTR-I with FKF

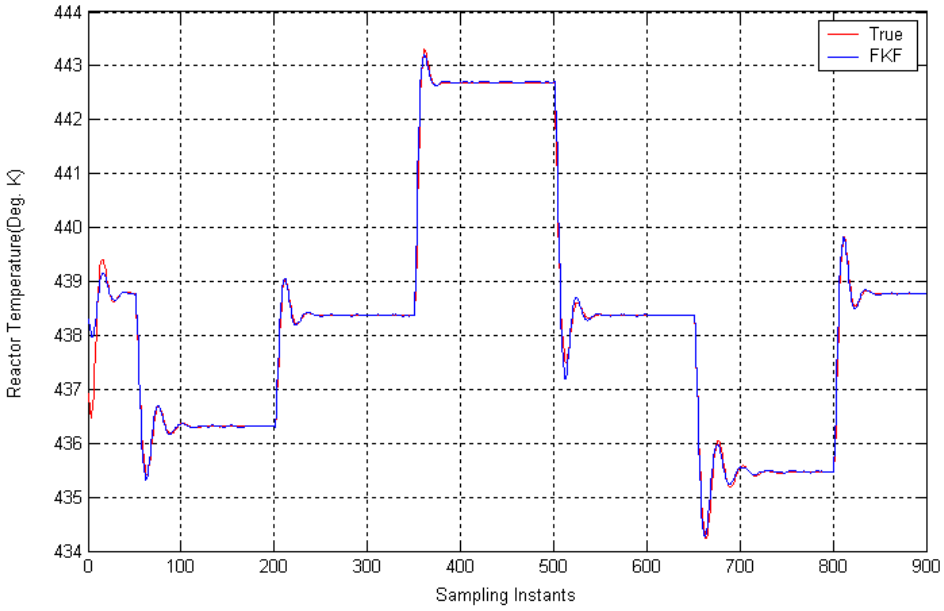

Figure 4.11 Evolution of true and estimated reactor temperature of CSTR-I with FKF

The initial value of the error covariance matrix $P(0/0)$ is assumed to be

$$P(0/0) = \begin{pmatrix} (0.05)^2 & 0 \\ 0 & (0.05)^2 \end{pmatrix}$$

for the FKF. From Figures 4.10 and 4.11, it can be concluded that reasonably good estimates of the reactor concentration and reactor temperature are obtained using FKF.

4.3.3 Augmented - state fuzzy Kalman filter for the CSTR-I process

In this sub-section, the performance of the ASFKF, in the presence of input disturbance is reported.

4.3.3.1 Input disturbance: state estimation in the presence of a step change in the feed temperature

In the previous sub-section, we assumed that the input disturbance variable (feed temperature) would remain at its nominal steady-state value. In this sub-section, the performance of the ASFKF, in the presence of a step change in the feed temperature, has been presented. By considering $\beta = T_o$ as an additional state (unmeasured) variable and augmenting the state space model, we obtain an equation of the form given by Equations (3.62) and (3.63). The model coefficient matrix Υ for different operating points is:

$$\Upsilon_1 = \begin{bmatrix} -1.3917 \text{x} 10^{-4} \\ 1.0366 \text{x} 10^{-1} \end{bmatrix} \qquad \Upsilon_2 = \begin{bmatrix} -1.4406 \text{x} 10^{-4} \\ 1.0451 \text{x} 10^{-1} \end{bmatrix}$$

$$\Upsilon_3 = \begin{bmatrix} -1.4857 \text{x} 10^{-4} \\ 1.0527 \text{x} 10^{-1} \end{bmatrix} \qquad \Upsilon_4 = \begin{bmatrix} -1.5264 \text{x} 10^{-4} \\ 1.0596 \text{x} 10^{-1} \end{bmatrix} \qquad \Upsilon_5 = \begin{bmatrix} -1.5264 \text{x} 10^{-4} \\ 1.0596 \text{x} 10^{-1} \end{bmatrix}$$

The C_η is chosen to be

$$C_\eta = [0]; \text{for } i = 1:5$$

The noise covariance matrix Q_β is assumed to be $6.25 \text{x} 10^{-2}$. The initial value of the additional state variable is chosen to be equal to the nominal steady-state value. Figures 4.12 to 4.14 show the estimated reactor concentration, the reactor temperature and the estimated unmeasured feed temperature in the CSTR-I for step changes in the feed temperature, random errors in measurement, and random fluctuations in the feed flow rate around the nominal value. From the responses, it can be concluded that the state estimates obtained using the ASFKF in the presence of step changes in the feed temperature, are reasonably good. The estimate of the feed temperature is determined to be reasonably accurate.

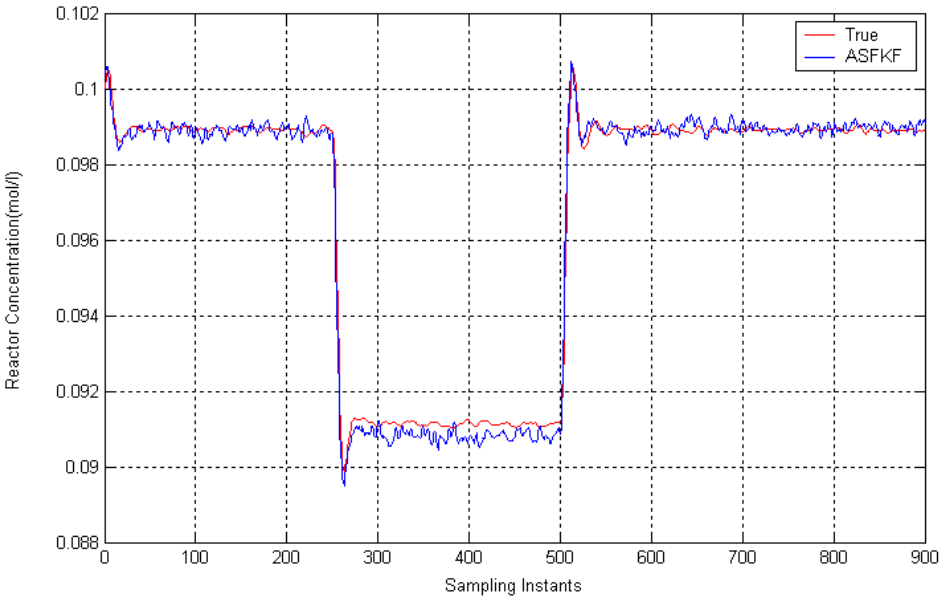

Figure 4.12 Evolution of true and estimated reactor concentration of CSTR-I with ASFKF (Input Disturbance)

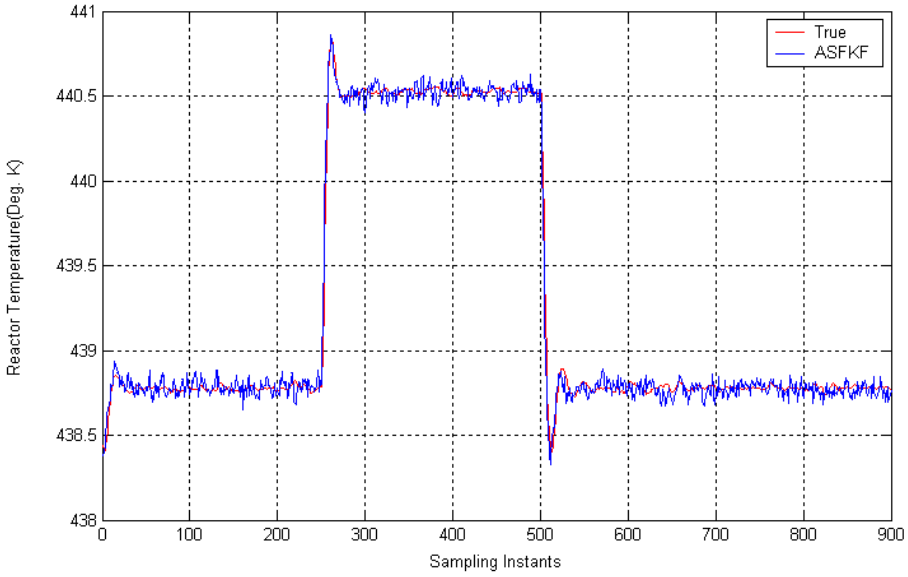

Figure 4.13 Evolution of true and estimated reactor temperature of CSTR-I with ASFKF (Input Disturbance)

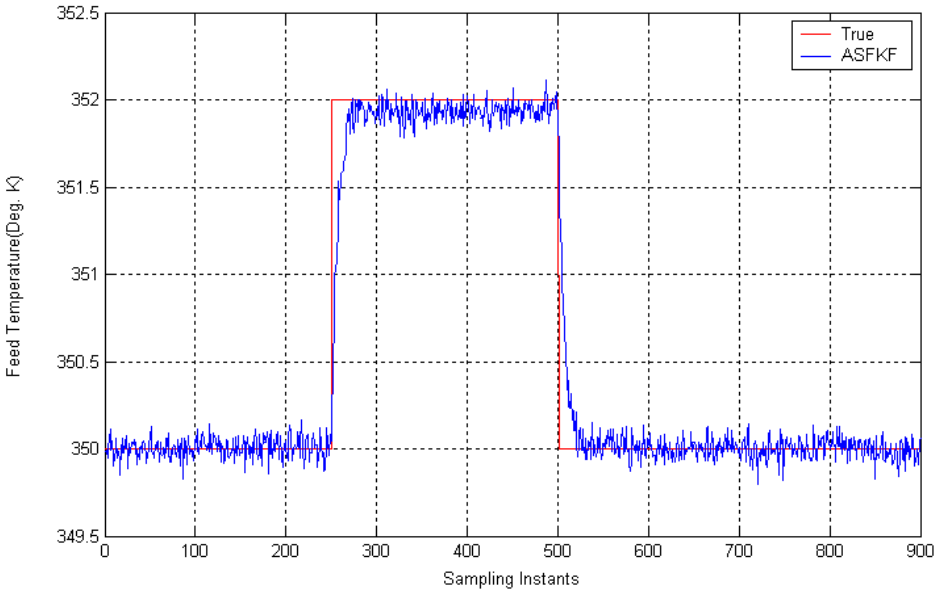

Figure 4.14 Evolution of true and estimated feed temperatures of CSTR-I with ASFKF

4.3.3.2 Output disturbance: state estimation in the presence of a bias in the temperature sensor

The performance of the FKF in the presence of a bias in the temperature sensor has been presented. By considering η as an additional state variable and augmenting the state space model, we obtain an equation of the form given by Equations (3.62) and (3.63). The model coefficient matrix has been chosen as

$$Y = \begin{bmatrix} 0 \\ 0 \end{bmatrix} \qquad \text{for } i = 1:5$$

$C_\eta = 1$. The noise covariance matrix Q_β is assumed to be 6.25 x10^{-4}. The initial value of the additional state variable is chosen to be equal to zero.

Figures 4.15 to 4.17 show the estimated reactor concentration, reactor temperature, and estimated value of the sensor bias in the CSTR-I in the presence of sensor bias of magnitude 0.5 K, as well as random errors in measurement and random fluctuations in the feed flow rate around the nominal value. Note that sensor bias with a magnitude of 0.5 K has been introduced as a step change in the first sampling instant. From the response, the estimate of the sensor bias (Refer Figure 4.17) is found to be reasonably accurate.

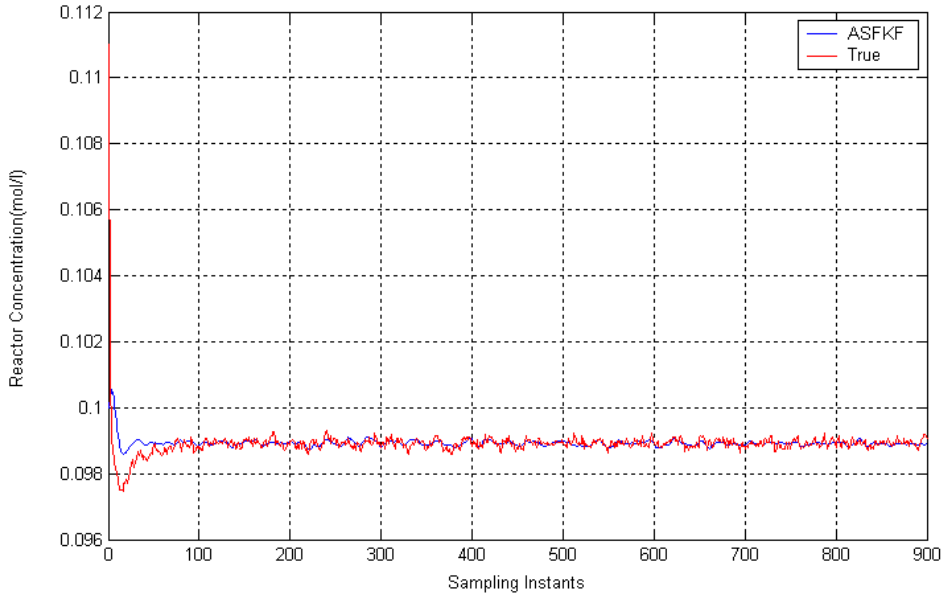

Figure 4.15 Evolution of true and estimated reactor concentration of CSTR-I with ASFKF (Output Disturbance)

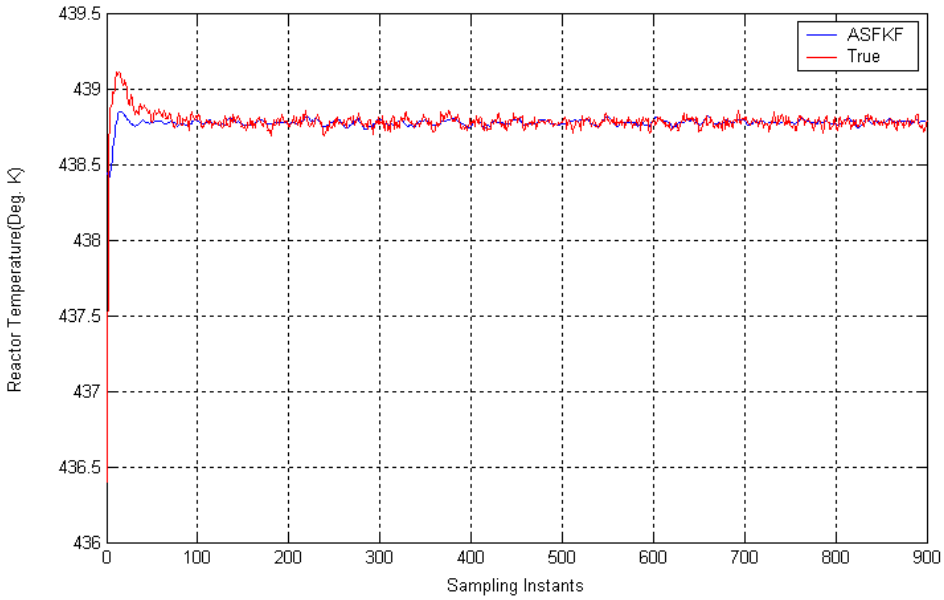

Figure 4.16 Evolution of true and estimated reactor temperature of CSTR-I with ASFKF (Output Disturbance)

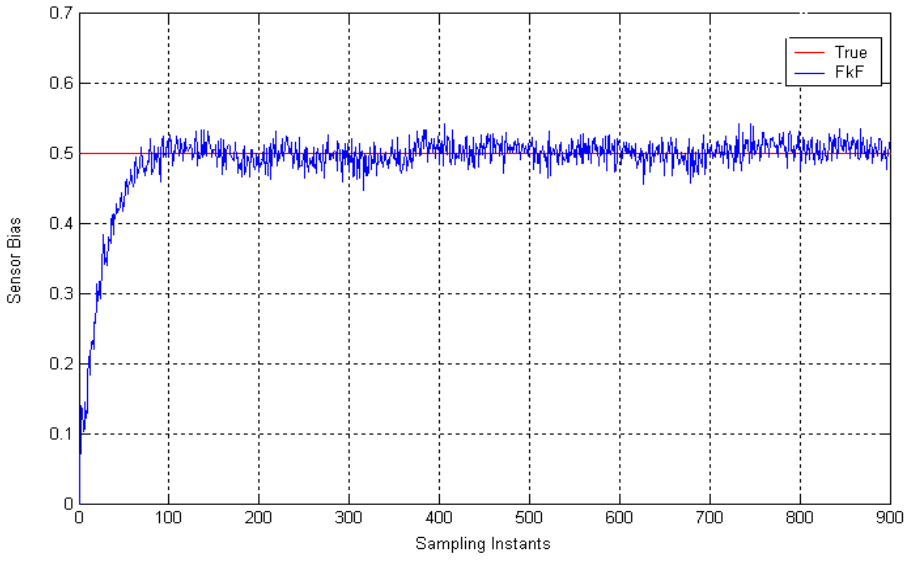

Figure 4.17 Evolution of sensor bias estimates of CSTR-I

4.4 OBSERVER FOR CSTR-II

4.4.1 FKF for CSTR-II process

The reactor temperature (premise variable) has been selected to partition the operating space of the CSTR-II system. Further, fuzzy sets described by membership functions on the domain of reactor temperature are used for partitioning the operating space of the system into overlapping regions. In this work, we have intended to interpolate three models generated at the three steady state operating points. Since, the operating space has been partitioned on a single parameter (reactor temperature) there are only three rules in the rule base. The universe of discourse is divided into three intervals defined by the linguistic variables low, medium and high respectively. Figure 4.18 shows the triangular membership functions that are used to partition the input space T. The linear time invariant discrete state space models for 3 different operating points have been obtained by discretising the continuous state space model equations (Refer Equations 4.3 and 4.4) with a sampling time equal to 0.1 hr.

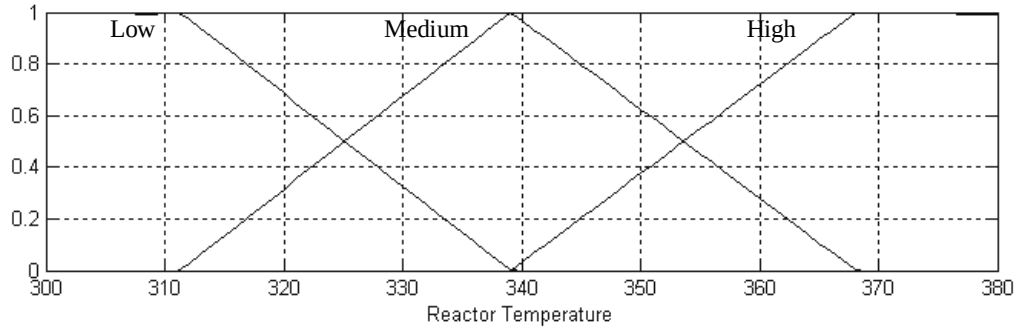

Figure 4.18 Membership function of CSTR-II

The discrete state space model parameters for different operating points of CSTR - II are:

Operating point: 1 (T=311.2 $\bar{C}_A$ = 8.564)

$$\Phi_1 = \begin{bmatrix} 0.8889 & -0.0083 \\ 0.1867 & 0.9750 \end{bmatrix}$$

$$\Gamma_1 = \begin{bmatrix} -0.0001 \\ 0.0296 \end{bmatrix}$$

Operating point:2 (T=339.1 $C_A = 5.518$)

$$\Phi_2 = \begin{bmatrix} 0.8238 & -0.0229 \\ 0.9526 & 1.1466 \end{bmatrix}$$

$$\Gamma_2 = \begin{bmatrix} -0.0003 \\ 0.0322 \end{bmatrix}$$

Operating point:3 (T=368.1 $C_A = 2.359$)

$$\Phi_3 = \begin{bmatrix} 0.6003 & -0.0311 \\ 3.5769 & 1.2438 \end{bmatrix}$$

$$\Gamma_3 = \begin{bmatrix} -0.0005 \\ 0.0338 \end{bmatrix}$$

$C = [0\ 1]$ (if T alone is measurable) for i=1:3

$$C = \begin{bmatrix} 1 & 0 \\ 0 & 1 \end{bmatrix}$$ (if both C_A and T are measurable) for i=1:3

In all the simulation runs, the process is simulated using the nonlinear first principles model (Refer Equations 4.5 and 4.6) and the true state variables are computed by solving the nonlinear differential equations using differential equation solver in Matlab 6.5. The simulation runs have been performed under the following initial conditions:

$$\text{Stable operating point}: C_A \,\&\, \hat{C}_A = 8.56 \quad T \,\&\, \hat{T} = 311.2$$

$$\text{Unstable operating point}: C_A \,\&\, \hat{C}_A = 5.518 \quad T \,\&\, \hat{T} = 339.1$$

The covariance matrices of measurement noise and state noise are assumed as:

$$R = \left[(0.05)^2 \right] \quad Q = \left[(0.05)^2 \right]$$

The initial value of the error covariance matrix $P(0/0)$ is assumed to be

$$P(0/0) = \begin{pmatrix} (0.05)^2 & 0 \\ 0 & (0.05)^2 \end{pmatrix}$$

The performance of the FKF to the variation in jacket temperature (Refer Figure 4.19), when only the reactor temperature alone is measured is shown in Figures 4.20 to 4.23. From Figures 4.20 to 4.23, it can be concluded that reasonably good estimates of the reactor concentration and reactor temperature are obtained using FKF both in stable and unstable operating points.

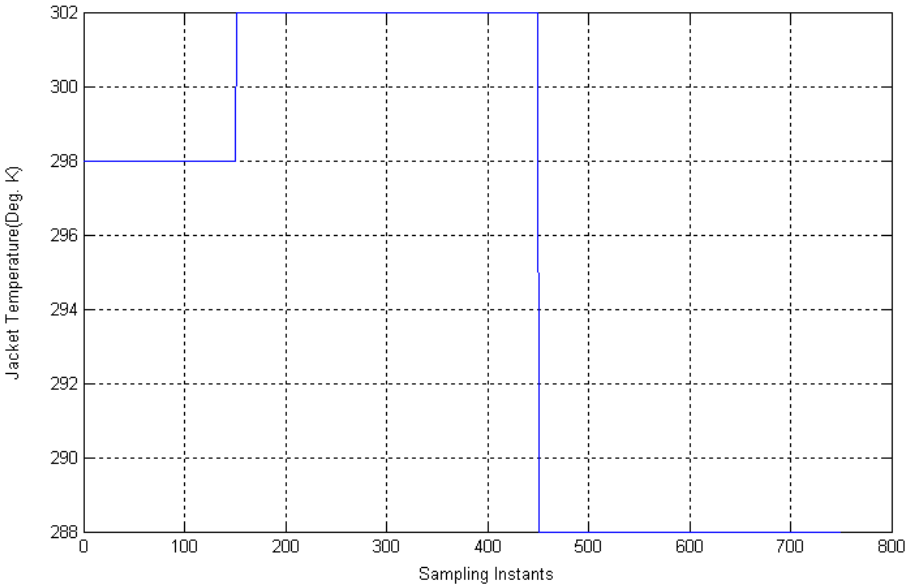

Figure 4.19 Variation in jacket temperature of CSTR-II

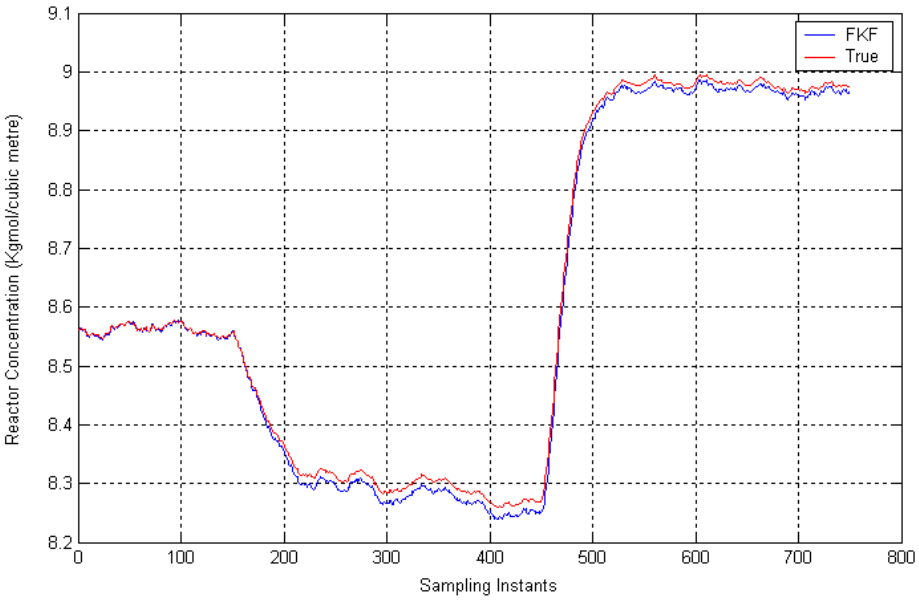

Figure 4.20 Evolution of true and estimated reactor concentration of CSTR-II with FKF (initial state of the process and estimator being at stable steady state)

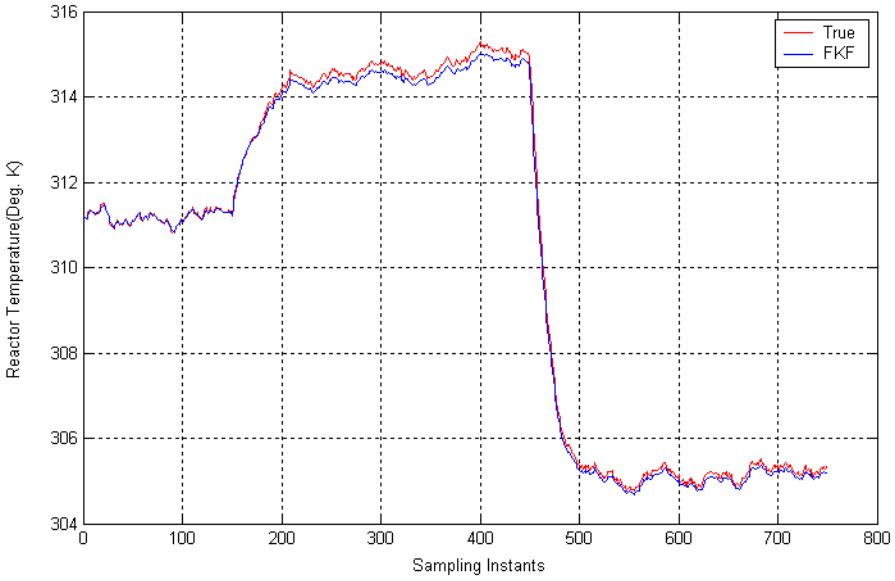

Figure 4.21 Evolution of true and estimated reactor temperature of CSTR-II with FKF (initial state of the process and estimator being at stable steady state)

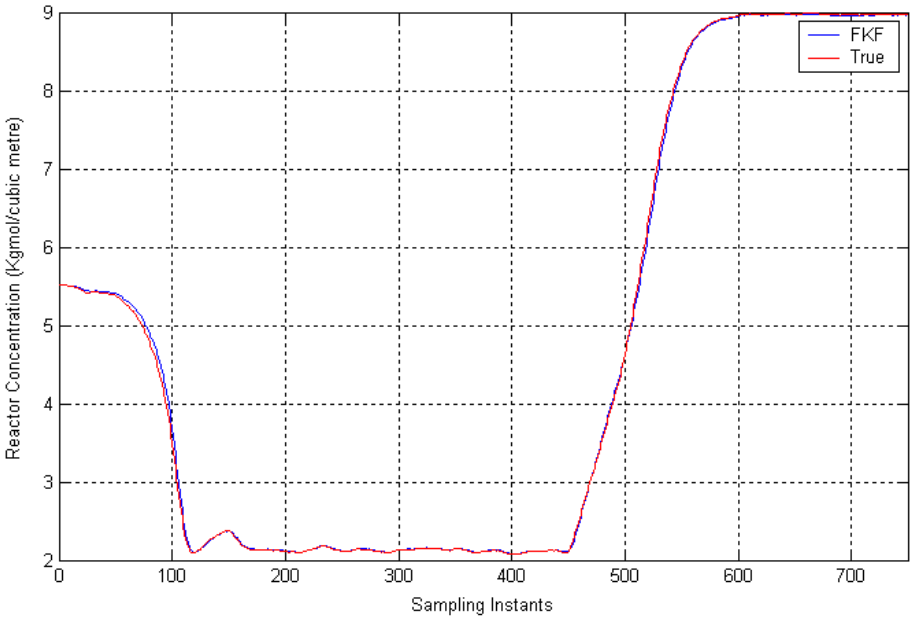

Figure 4.22 Evolution of true and estimated reactor concentration of CSTR-II with FKF (initial state of the process and estimator being at unstable steady state)

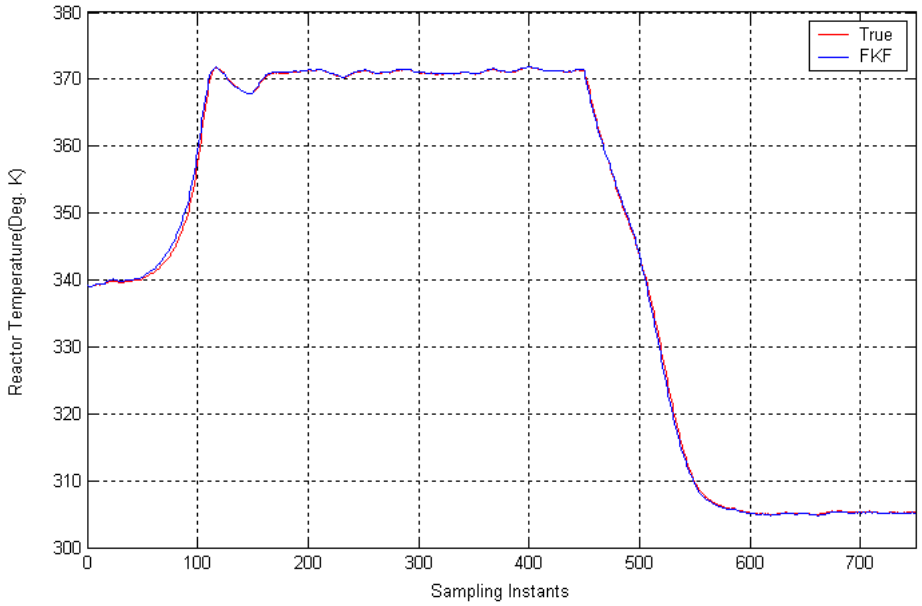

Figure 4.23 Evolution of true and estimated reactor temperature of CSTR-II with FKF (initial state of the process and estimator being at unstable steady state)

4.5 COMPARISON OF FUZZY KALMAN FILTER AND EXTENDED KALMAN FILTER

The performance of the proposed nonlinear state estimation scheme has to be assessed through simulation because we are dealing with stochastic systems. For each case that is being analyzed, a simulation run consisting of N_T trials with length of each simulation trail being equal to L is conducted. In all the simulation trials, the sum of square of the estimation errors, which is nothing but the difference between the true value of the state variables and the estimated value of the state variables, has been obtained.

The mean and standard deviation of the estimation error based on 25 Monte Carlo simulations for FKF and EKF are reported in Table 4.4. For

FKF and EKF identical realization of state and measurement noises have been used in all the simulation trails. From Table 4.4, it can be observed that the estimates obtained by FKF are as good as those obtained by the EKF in all the cases. The evolution of true and estimated reactor concentration and reactor temperature of CSTR-I with EKF and FKF for a simulation trail are shown in Figures 4.24 and 4.25. From the Figures 4.24 and 4.25, it can be concluded that FKF performance is similar to that of EKF.

The FKF helps to reduce the number of computations needed compared to the conventional EKF. That is, in the EKF, for each time k, all the system matrices must be calculated using the related jacobians as well as the updated state estimates at time k. Also, in EKF the nonlinear differential equations have to be numerically integrated to obtain the predicted estimates of the state variables. On the other hand, in FKF although more matrices are needed, all of them have constant values limiting the calculation to

- The determination of weights that will be provided by the membership functions.
- State propagation calculations of each model using the appropriate matrices and weighted average of the local linear model outputs.

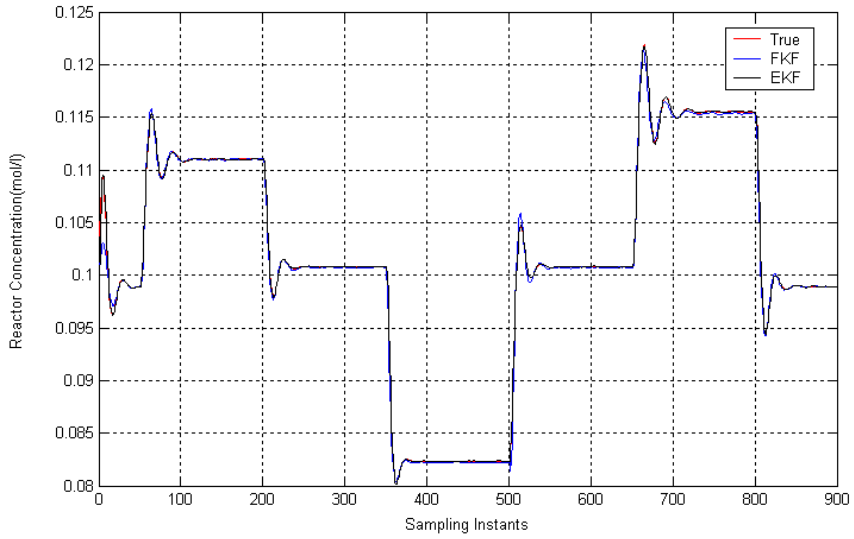

Figure 4.24 Evolution of true and estimated reactor concentration of CSTR-I with FKF and EKF

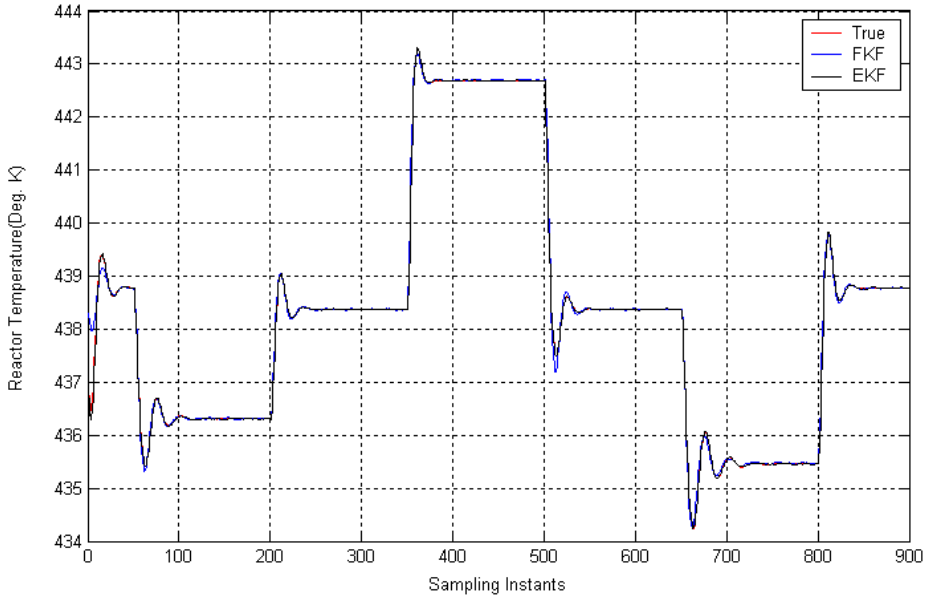

Figure 4.25 Evolution of true and estimated reactor temperature of CSTR-I with FKF and EKF

Table 4.4 Estimation error for 25 Monte-Carlo simulations

Measurements	Fuzzy Kalman filter				Extended Kalman Filter			
	C_A		T		C_A		T	
	μ	σ	μ	σ	μ	σ	μ	σ
C_A and T	2.7768e-04	2.6025e-06	11.6628	0.1472	1.9127e-04	3.577e-05	9.8652	1.9190
T only	2.7845e-04	2.6134e-06	11.6897	0.1475	1.9214e-04	3.5931e-05	9.8943	1.9246

Since, it is not necessary to calculate jacobians and numerical integration of nonlinear differential equation, the proposed FKF approach has better implementation capabilities to the EKF.

In order to test the efficacy of the EKF and FKF algorithms, the computation time per sampling instant in a single simulation trail (length of the simulation trail is 900) has been presented in the form of histogram. From the Figure 4.26 it can be concluded that the computation time per sampling instant of FKF algorithm is always less than 0.01 second, whereas for EKF algorithm, it falls between 0.05 and 0.1 seconds (Refer Figure 4.27). The computation time per sampling instant of the FKF for the system considered for simulation study has been found to be negligible. It should be noted that the computation time of FKF for even higher order problems will be always less demanding as compared with that of EKF.

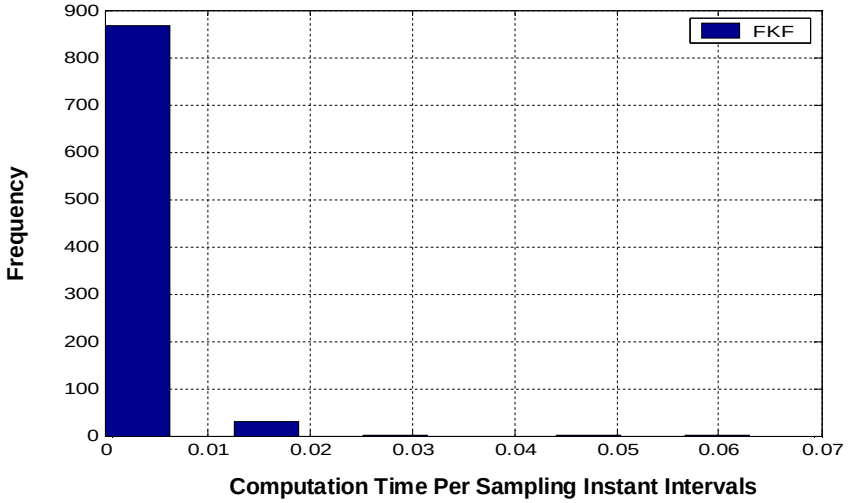

Figure 4.26 Histogram of CSTR-I computation time per sampling instant - FKF

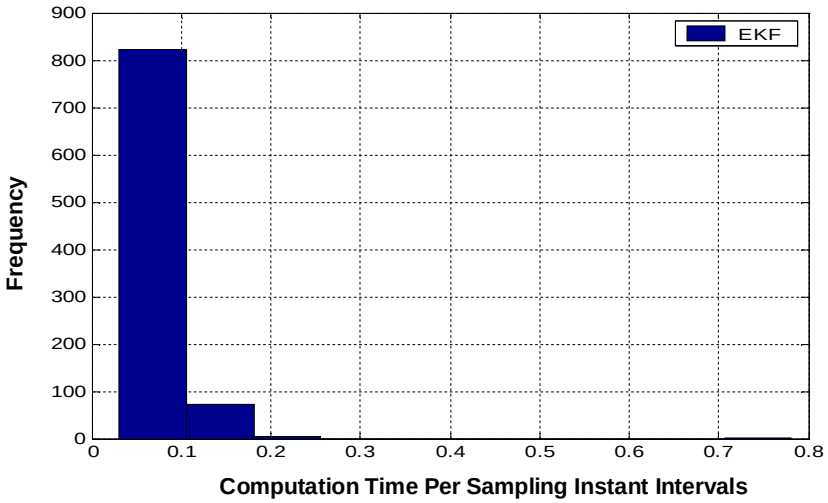

Figure 4.27 Histogram of CSTR-I computation time per sampling instant - EKF